




Improved electrochemical performance of SiO₂-coated Li-rich layered oxides-Li_{1.2}Ni_{0.13}Mn_{0.54}Co_{0.13}O₂

Jeffin James Abraham¹, Umair Nisar¹, Haya Monawwar², Aisha Abdul Quddus³, R. A. Shakoor^{1,*} , Mohamed I. Saleh¹, Ramazan Kahraman³, Siham Al-Qaradawi⁴, and Amina S. Aljaber⁴

¹Center for Advanced Materials (CAM), Qatar University, Doha, Qatar

²Department of Electrical Engineering, College of Engineering, Qatar University, Doha, Qatar

³Department of Chemical Engineering, College of Engineering, Qatar University, Doha, Qatar

⁴Department of Chemistry & Earth Sciences, College of Arts and Science, Qatar University, P.O. Box 2713, Doha, Qatar

Received: 18 May 2020

Accepted: 11 September 2020

Published online:

29 September 2020

© The Author(s) 2020

ABSTRACT

Lithium-rich layered oxides (LLOs) such as Li_{1.2}Ni_{0.13}Mn_{0.54}Co_{0.13}O₂ are suitable cathode materials for future lithium-ion batteries (LIBs). Despite some salient advantages, like low cost, ease of fabrication, high capacity, and higher operating voltage, these materials suffer from low cyclic stability and poor capacity retention. Several different techniques have been proposed to address the limitations associated with LLOs. Herein, we report the surface modification of Li_{1.2}Ni_{0.13}Mn_{0.54}Co_{0.13}O₂ by utilizing cheap and readily available silica (SiO₂) to improve its electrochemical performance. Towards this direction, Li_{1.2}Ni_{0.13}Mn_{0.54}Co_{0.13}O₂ was synthesized utilizing a sol-gel process and coated with SiO₂ (SiO₂ = 1.0 wt%, 1.5 wt%, and 2.0 wt%) employing dry ball milling technique. XRD, SEM, TEM, elemental mapping and XPS characterization techniques confirm the formation of phase pure materials and presence of SiO₂ coating layer on the surface of Li_{1.2}Ni_{0.13}Mn_{0.54}Co_{0.13}O₂ particles. The electrochemical measurements indicate that the SiO₂-coated Li_{1.2}Ni_{0.13}Mn_{0.54}Co_{0.13}O₂ materials show improved electrochemical performance in terms of capacity retention and cyclability when compared to the uncoated material. This improvement in electrochemical performance can be related to the prevention of electrolyte decomposition when in direct contact with the surface of charged Li_{1.2}Ni_{0.13}Mn_{0.54}Co_{0.13}O₂ cathode material. The SiO₂ coating thus prevents the unwanted side reactions between cathode material and the electrolyte. 1.0 wt% SiO₂-coated Li_{1.2}Ni_{0.13}Mn_{0.54}Co_{0.13}O₂ shows the best electrochemical performance in terms of rate capability and capacity retention.

Address correspondence to E-mail: shakoor@qu.edu.qa

1 Introduction

The energy storage requirements have been stringent throughout the years, and Li-ion batteries (LIBs) are an ideal solution that has been leading this field owing to their higher energy and power density [1–4]. With environmental concerns, there have been increasing interest in renewable energy sources [3]. The energy generated from various renewable energy sources must be stored into energy storage devices which could supply them instantly when needed [1]. In this regard, LIBs are considered the most attractive and viable option due to their higher energy and power density capabilities [2, 5]. LIBs are being used as power sources for most of the portable devices that we use in our daily life. However, to fulfill future demands for electric vehicles (EVs) and large scale energy storage system (ESS), the development of new materials with improved performance is essential [2, 5]. Since the commercialization of lithium-ion batteries by Sony in 1991, there has been no significant breakthrough in the development of new cathode materials [1, 6]. With more interest in electric vehicles, there is a severe need for new cathode materials with enhanced energy and power density, a stable and long cycle life, and with improved safety [7–11].

Lithium-rich layered oxides (LLOs) cathodes display a promising performance in terms of capacity and operating voltage and hence is considered as a potential cathode for future lithium-ion batteries. These materials have already gained much attention previously because of their considerably high discharge capacities ($> 250 \text{ mAh g}^{-1}$) and higher operating voltages [12–18]. These materials are also very cost-effective and easy to produce [19, 20]. However, despite the tempting characteristics, these materials have a few drawbacks that need to be addressed before successful commercialization. These materials experience rapid capacity and voltage fading during successive cycles that have an adverse effect on their energy density. Moreover, these materials also experience poor rate capability and have serious safety concerns [18, 21–26].

To overcome these issues, various optimization techniques such as surface modification, doping of transition metals and morphology control have been widely reported [11, 18, 27]. Among them, the surface coating is widely accepted by the battery community

for improving the performance of cathode materials for lithium-ion batteries [10, 11]. The surface coatings help to prevent the direct contact of electrolyte and the cathode material, thereby, reducing the unwanted side reactions by electrolyte oxidation, especially at higher operating voltages [28–34]. The type of coating and the coating thickness largely affects the overall performance of cathode materials. Thin and homogeneous coatings are ideal for the ultimate performance. However, if the coating is thick, it may impede the lithium-ion movement, which leads to an increase in charge transfer resistance at the cathode/electrolyte interface leading to inferior electrochemical performance [35, 36]. Several coating materials have been proposed and reported [37–39]. Among them, SiO_2 is readily available, cheap and environmentally friendly material [40–43]. However, it is challenging to develop a homogenous SiO_2 coating on the surface of particles since it requires high heat treatment temperatures and additional heat treatment step, which significantly increase the processing cost.

Here, we report the in situ coating process without any additional heat treatment step to form a homogeneous SiO_2 coating layer. The process itself is viable, scalable and cheap without employing any additional heat treatment step, making it as an ideal candidate for the coating material. Recently, there have been few reports on SiO_2 coating for cathode materials which show promising electrochemical results [11]. Herein, we synthesized and characterized SiO_2 -coated $\text{Li}_{1.2}\text{Ni}_{0.13}\text{Mn}_{0.54}\text{Co}_{0.13}\text{O}_2$ ($\text{SiO}_2 = 1.0, 1.5$ and $2.0 \text{ wt}\%$). The $\text{Li}_{1.2}\text{Ni}_{0.13}\text{Mn}_{0.54}\text{Co}_{0.13}\text{O}_2$ (LLO) was prepared by the sol-gel synthesis process and coated with SiO_2 using dry ball milling approach. The phase purity of the synthesized materials was analyzed using X-ray diffraction (XRD) technique. The particle morphology was investigated using scanning and transmission electron microscopes (SEM and TEM). TEM was further used for elemental mapping of the synthesized materials. X-ray photoelectron spectroscopy (XPS) was used to identify the chemical states of different elements present in the cathode materials. Finally, the electrochemical measurements were conducted, and the performance of uncoated and SiO_2 -coated $\text{Li}_{1.2}\text{Ni}_{0.13}\text{Mn}_{0.54}\text{Co}_{0.13}\text{O}_2$ ($\text{SiO}_2 = 1.0, 1.5$ and $2.0 \text{ wt}\%$) materials was compared to elucidate the beneficial role of SiO_2 coatings.

2 Experimental

2.1 Materials preparation

The $\text{Li}_{1.2}\text{Ni}_{0.13}\text{Mn}_{0.54}\text{Co}_{0.13}\text{O}_2$ was prepared using sol-gel synthesis process. The stoichiometric amounts of lithium acetate, manganese acetate, cobalt acetate, and nickel acetate (1.2:0.54:0.13:0.13) were added to 100 ml distilled water at 60 °C with continuous stirring. All the precursors were purchased from Sigma Aldrich. Later citric acid was added to the precursor solution in the ratio 1:2 (citric acid: metal ions) which acted as the chelating agent. Under constant stirring, the solution temperature was increased to 80 °C and left until a gel was formed. The gel was transferred to the oven at 120 °C to remove the traces of water from the gel. After complete drying, the gel was then ground into a fine powder, pressed into pellets, and decomposed in a muffle furnace at 450 °C for 6 h. The decomposed precursor material was again grounded using an agate mortar and mixed homogenously. Finally, the precursor material was again pressed into pellets and calcined at 900 °C for 12 h in the muffle furnace to get the desired material.

The SiO_2 -coated $\text{Li}_{1.2}\text{Ni}_{0.13}\text{Mn}_{0.54}\text{Co}_{0.13}\text{O}_2$ (SiO_2 = 1.0, 1.5 and 2.0 wt%) materials were synthesized by a similar synthesis process as above stated. However, after decomposition of the precursor at 450 °C for 6, SiO_2 nanoparticles were added to it and ball milled for 24 h using zirconia balls. Later, this material was calcined at 900 °C for 12 h to achieve SiO_2 -coated materials. Figure 1 shows the experimental process for the synthesis of the $\text{Li}_{1.2}\text{Ni}_{0.13}\text{Mn}_{0.54}\text{Co}_{0.13}\text{O}_2$ cathode materials.

2.2 Structural, compositional, and thermal stability characterization

Powder X-ray diffraction analysis (PAN Analytical—Empyrean) with Cu-K α radiation (1.5425 Å) was used to analyze the phase purity and study the crystal structure of the synthesized materials. The samples were scanned in the range $10 \leq 2\theta \leq 90^\circ$ with a scan step size of 0.01313° . Field emission scanning electron microscopy (FE-SEM) and transmission electron microscopy (TEM) were used to investigate the particle morphology. TEM was further used for elemental mapping of the surfaces of the synthesized materials. X-ray photoelectron spectroscopy (XPS,

Thermo-Scientific-Sigma Probe) was further used to confirm the presence of SiO_2 coating layer on the particle surface and to study the chemical states of different elements in synthesized materials. Furthermore, surface area and porosity of the developed materials were analyzed using BET (Quanta chrome 4200e) technique. Thermal stability of pristine and SiO_2 -coated $\text{Li}_{1.2}\text{Ni}_{0.13}\text{Mn}_{0.54}\text{Co}_{0.13}\text{O}_2$ materials was studied using DSC, 8500, PerkinElmer. For DSC measurement, the cells were charged to 4.7 V at 0.1 C and transferred to the argon-filled glovebox. The cells were opened, and the excessive electrolyte was removed from the electrode surface. The electrode was scratched from the current aluminum collector and transferred to the high-pressure stainless-steel pan. DSC measurements were performed from room temperature to 450 °C with a heating rate of 5 °C.

2.3 Electrode and cell fabrication

Electrode fabrication for electrochemical testing was done by forming a slurry of the active materials (uncoated and SiO_2 -coated $\text{Li}_{1.2}\text{Ni}_{0.13}\text{Mn}_{0.54}\text{Co}_{0.13}\text{O}_2$), Super-P carbon, and PVDF binder in the ratio 80:10:10 respectively in the NMP solvent. The cathode slurry was mixed in a glass vial for around 12 h. Later, this slurry was coated on aluminum current collect using the doctor blade, keeping the thickness of the coated electrode around 25 μm . The cast electrode was then shifted to the oven for drying at 120 °C for 3 h. The electrodes were then calendared using a rolling press. Electrodes with a diameter of 14 mm were then punched from the calendared electrodes. These circular electrodes were shifted to a vacuum oven at 120 °C for 2 h to remove the trace of water. Finally, the electrodes were moved to an argon-filled glovebox for cell fabrication. For electrochemical testing, CR-2032 coin cells were fabricated using lithium metal as the anode, and 1 M LiPF_6 in a mixture of dimethyl carbonate (DMC) and ethylene carbonate (EC) (1:1 by v/v.) (Sigma Aldrich) was used as an electrolyte. Moreover, Celgard 2325 was used as the separator. The electrochemical tests for these materials were conducted at room temperature (25 °C) using WonAtech (WBCS 3000L, Korea) battery cycler. All the galvanostatic charge/discharge measurement were conducted in the voltage window of 2.0–4.9 V.

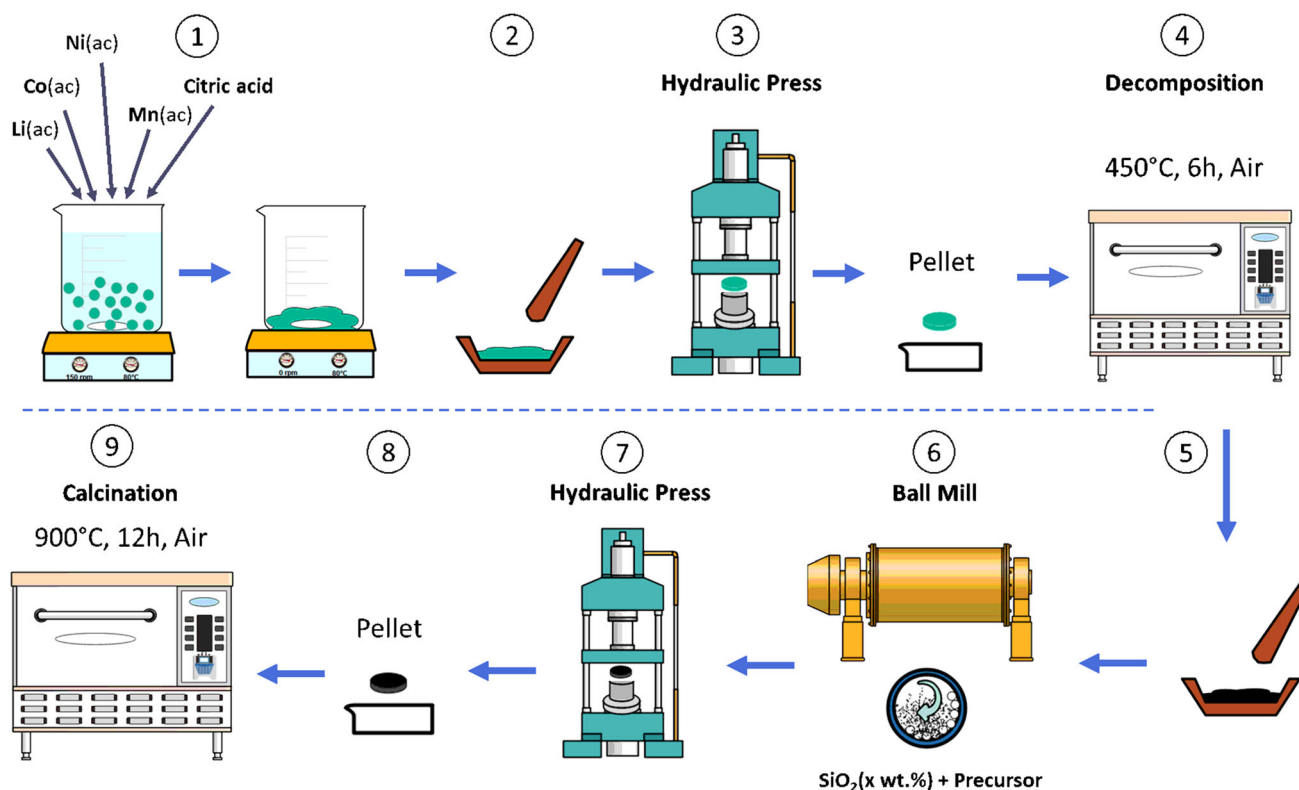


Fig. 1 A diagram illustrating the experimental process to synthesize uncoated and SiO_2 -coated $\text{Li}_{1.2}\text{Ni}_{0.13}\text{Mn}_{0.54}\text{Co}_{0.13}\text{O}_2$ ($\text{SiO}_2 = 1.0, 1.5$ and 2.0 wt%) materials

3 Results and discussion

XRD spectra of uncoated and SiO_2 -coated $\text{Li}_{1.2}\text{Ni}_{0.13}\text{Mn}_{0.54}\text{Co}_{0.13}\text{O}_2$ ($\text{SiO}_2 = 1.0, 1.5$ and 2.0 wt%) materials are shown in Fig. 2. XRD spectra confirmed the synthesis of highly crystalline materials without the

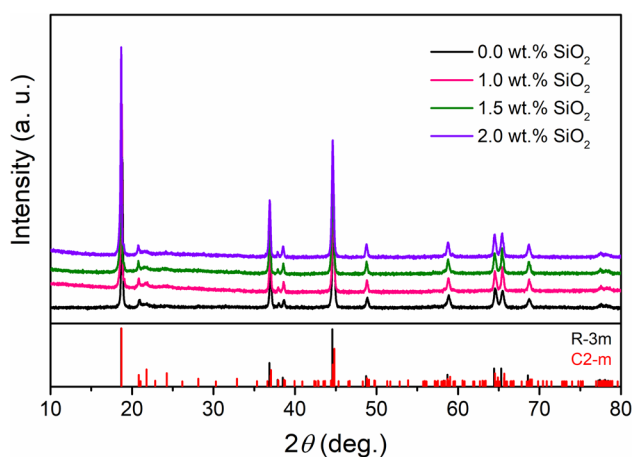
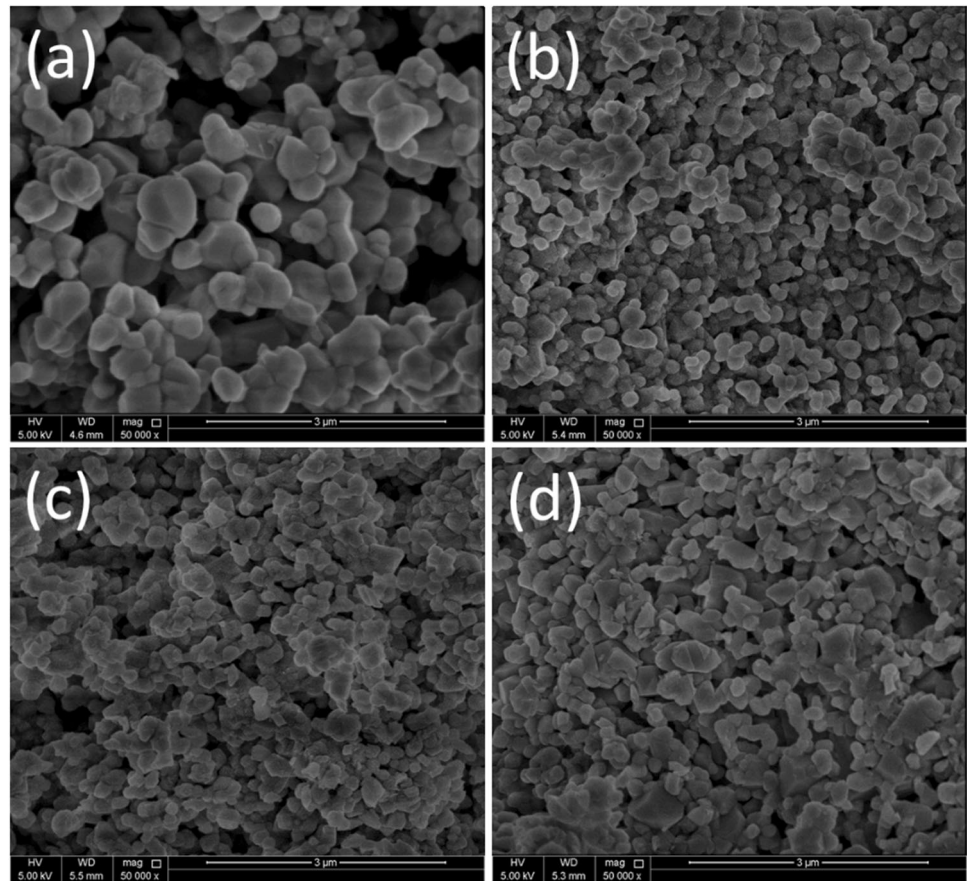


Fig. 2 XRD spectra of uncoated and SiO_2 -coated $\text{Li}_{1.2}\text{Ni}_{0.13}\text{Mn}_{0.54}\text{Co}_{0.13}\text{O}_2$ ($\text{SiO}_2 = 1.0, 1.5$ and 2.0 wt%) materials

presence of any impurity phases. The synthesized materials are indexed to R-3m and C2/m space groups, as reported earlier [19, 44]. Furthermore, it can be noticed that there is no significant difference between the XRD spectra of uncoated and SiO_2 -coated $\text{Li}_{1.2}\text{Ni}_{0.13}\text{Mn}_{0.54}\text{Co}_{0.13}\text{O}_2$ materials. Finally, due to the presence of a small amount of SiO_2 , it is undetected using XRD analysis.

The FE-SEM images of the uncoated and SiO_2 -coated $\text{Li}_{1.2}\text{Ni}_{0.13}\text{Mn}_{0.54}\text{Co}_{0.13}\text{O}_2$ ($\text{SiO}_2 = 1.0, 1.5$ and 2.0 wt%) materials are displayed in Fig. 3. It is observed that all synthesized materials display a well-defined morphology with homogenous particle size distribution. It can also be observed that the particle size for the SiO_2 -coated $\text{Li}_{1.2}\text{Ni}_{0.13}\text{Mn}_{0.54}\text{Co}_{0.13}\text{O}_2$ ($\text{SiO}_2 = 1.0, 1.5$ and 2.0 wt%) materials is smaller when compared with the uncoated sample which can be due to the ball milling effect. The average particle size for uncoated $\text{Li}_{1.2}\text{Ni}_{0.13}\text{Mn}_{0.54}\text{Co}_{0.13}\text{O}_2$ is $\sim 400\text{--}800$ nm, whereas the average particle size for SiO_2 -coated $\text{Li}_{1.2}\text{Ni}_{0.13}\text{Mn}_{0.54}\text{Co}_{0.13}\text{O}_2$ is $\sim 150\text{--}350$ nm. The particle size of the developed materials was calculated using ImageJ software. The

Fig. 3 FE-SEM images of **a** uncoated and **b–d** SiO₂-coated Li_{1.2}Ni_{0.13}Mn_{0.54}Co_{0.13}O₂ (SiO₂ = 1.0, 1.5 and 2.0 wt%) materials



reduction in particle size of the coated materials can be due to (i) dry ball milling effect and (ii) impediment of particle growth at high-temperature calcination owing to the presence of SiO₂ coating on the particle surface. The BET curves for the uncoated and SiO₂-coated Li_{1.2}Ni_{0.13}Mn_{0.54}Co_{0.13}O₂ materials are shown in Fig. S-1. No significant difference can be found in BET isotherms for uncoated, and SiO₂-coated Li_{1.2}Ni_{0.13}Mn_{0.54}Co_{0.13}O₂ materials. The surface area for uncoated material is 6.139 m²/g whereas the coated materials have 6.718 m²/g, 6.412 m²/g and 6.120 m²/g for 1.0 wt, 1.5 wt and 2.0 wt% SiO₂, respectively.

High-resolution TEM and element mapped images for 1.5 wt% SiO₂-coated Li_{1.2}Ni_{0.13}Mn_{0.54}Co_{0.13}O₂ are shown in Fig. 4. Figure 4a clearly shows the rock-like spherical morphology of the particles. The particle size of 1.5 wt% SiO₂-coated Li_{1.2}Ni_{0.13}Mn_{0.54}Co_{0.13}O₂ samples is ~ 150–300 nm which is consistent with FE-SEM images in Fig. 3. TEM image of 1.5 wt% SiO₂-coated Li_{1.2}Ni_{0.13}Mn_{0.54}Co_{0.13}O₂ material shown in Fig. 4b confirms the existence of the SiO₂ coating layer on the particles. Furthermore, TEM elemental

mapping of SiO₂-coated Li_{1.2}Ni_{0.13}Mn_{0.54}Co_{0.13}O₂ materials was also conducted, and the results for 1.5 wt% coated Li_{1.2}Ni_{0.13}Mn_{0.54}Co_{0.13}O₂ are shown in Fig. 4c–h. The homogenous distribution of Ni, Mn, Co, O, and Si on the particle surfaces can be identified from elemental mapping images which further confirms the presence of Si on the particle surfaces. It is pertinent to note that SiO₂ is homogeneously coated on the surface of the particles even with small amounts used. Hence, both high-resolution TEM and elemental mapping images provide strong evidence for the existence of a homogeneous SiO₂ coating around the particles of Li_{1.2}Ni_{0.13}Mn_{0.54}Co_{0.13}O₂, which is expected to have a positive impact on its electrochemical properties.

XPS analysis was performed on uncoated and SiO₂-coated Li_{1.2}Ni_{0.13}Mn_{0.54}Co_{0.13}O₂ to study the chemical states of transition metals in the synthesized materials and further to get evidence of SiO₂ layer on the Li_{1.2}Ni_{0.13}Mn_{0.54}Co_{0.13}O₂ surface as shown in Fig. 5. The survey patterns for the uncoated and SiO₂-coated Li_{1.2}Ni_{0.13}Mn_{0.54}Co_{0.13}O₂ (SiO₂ = 1.0, 1.5 and 2.0 wt%) materials are shown in Fig. S-2. The high-resolution

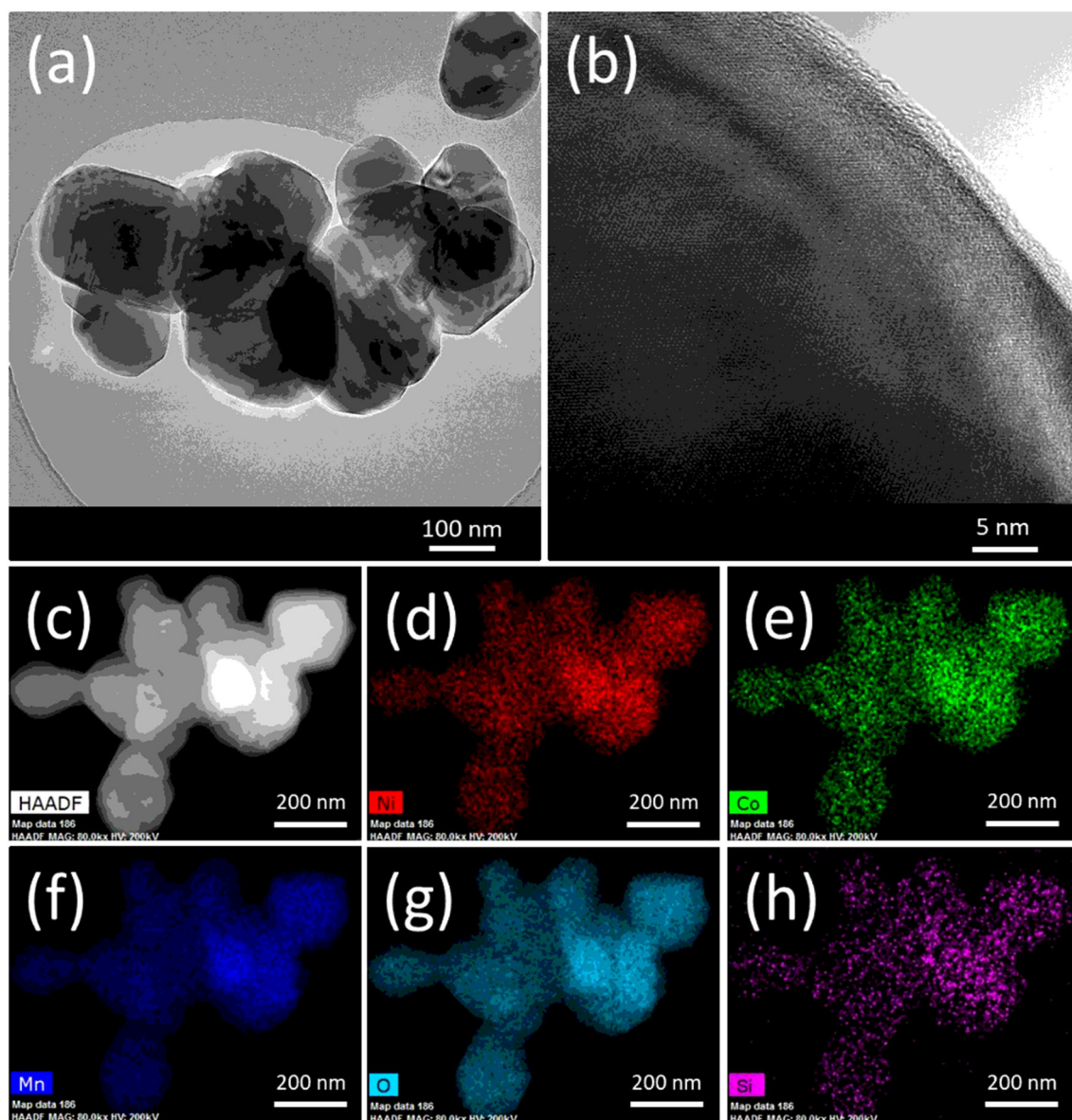


Fig. 4 a–b TEM images c–h elemental mapping images for 1.5 wt% SiO₂-coated Li_{1.2}Ni_{0.13}Mn_{0.54}Co_{0.13}O₂ materials

XPS spectra for Si further confirmed the presence of SiO₂ coating layer. The XPS spectra were fitted using XPS peaks fit software to analyze the chemical states of the transition metals. The high-resolution spectra for Si (Fig. 5m–p) clearly show that no SiO₂ layer was present on uncoated Li_{1.2}Ni_{0.13}Mn_{0.54}Co_{0.13}O₂, whereas, for the coated materials, the SiO₂ can be detected. The high-resolution XPS spectra for Ni, as shown in Fig. 5a–d display two peaks as Ni2p_{1/2} at 872.77 ± 0.20 eV and Ni2p_{3/2} at 854.82 ± 0.10 eV, which corresponds to Ni²⁺ [18]. Moreover, as shown in Fig. 5e–h, Mn shows peaks for Mn2p_{1/2} at 654.42 ± 0.28 eV and Mn2p_{3/2} at 642.66 ± 0.10 eV,

which is consistent with the presence of Mn⁴⁺ [29, 45]. Finally, Co also displays two peaks as Co2p_{1/2} at 795.68 ± 0.11 eV and Co2p_{3/2} at 780.68 ± 0.1 eV, as shown in Fig. 5i–l, which corresponds to Co³⁺. The binding energies for the transition metals are displayed in Table 1, which are consistent with previous reports [29, 45]. It can be noticed that with the increasing amount of SiO₂ as coating, there is a slight increase in the binding energies of Si, which may be due to stronger interactions of SiO₂ with Li_{1.2}Ni_{0.13}Mn_{0.54}Co_{0.13}O₂ materials.

The galvanostatic charge/discharge curves of uncoated and SiO₂-coated Li_{1.2}Ni_{0.13}Mn_{0.54}Co_{0.13}O₂

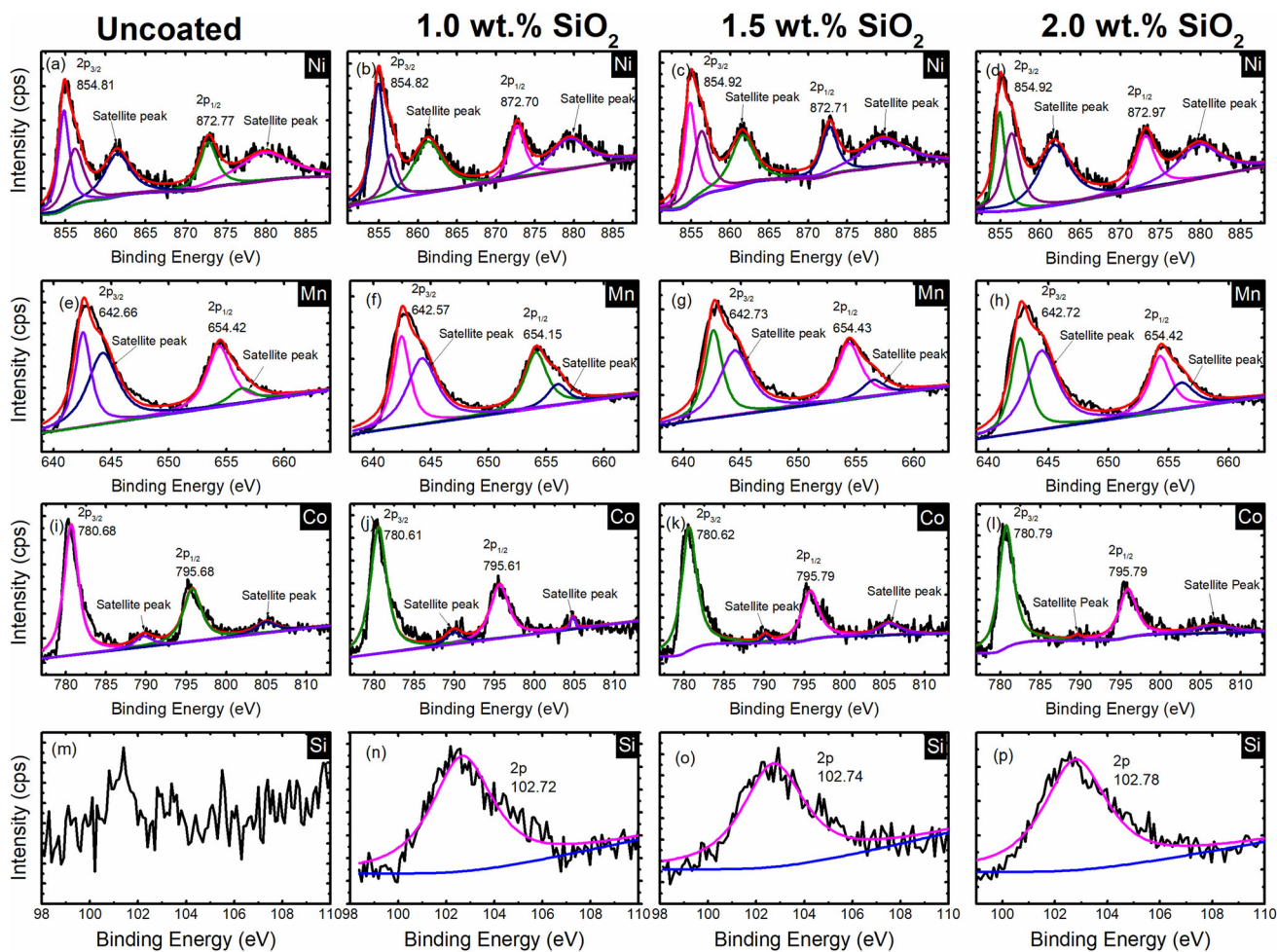


Fig. 5 XPS spectra of uncoated and SiO₂-coated Li_{1.2}Ni_{0.13}Mn_{0.54}Co_{0.13}O₂ (SiO₂ = 1.0, 1.5 and 2.0 wt%) materials

Table 1 Binding energies of metals in uncoated and SiO₂-coated

Li_{1.2}Ni_{0.13}Mn_{0.54}Co_{0.13}O₂

Material	Mn		Ni		Co		Si
	2p _{3/2}	2p _{1/2}	2p _{3/2}	2p _{1/2}	2p _{3/2}	2p _{1/2}	2p
0.0 wt% SiO ₂	642.66	654.42	854.81	872.77	780.68	795.68	–
1.0 wt% SiO ₂	642.57	654.15	854.82	872.70	780.61	795.61	102.72
1.5 wt% SiO ₂	642.73	654.43	854.92	872.71	780.62	795.79	102.74
2.0 wt% SiO ₂	642.72	654.42	854.92	872.97	780.79	795.79	102.78
Ref. [29, 45]	642.7	654.10	855.00	872.30	780.80	795.20	–

(SiO₂ = 1.0, 1.5 and 2.0 wt%) materials at various C-rates are shown in Fig. 6. For the uncoated material, the discharge capacities are ~ 205 mAh g⁻¹ and 16 mAh g⁻¹ at 0.1 C and 2 C, respectively. Whereas SiO₂-coated Li_{1.2}Ni_{0.13}Mn_{0.54}Co_{0.13}O₂ (SiO₂ = 1.0, 1.5 and 2.0 wt%) materials show similar initial discharge capacities but demonstrate better discharge capacity, especially at higher C-rates. For instance, the 1.0 wt% SiO₂-coated Li_{1.2}Ni_{0.13}Mn_{0.54}Co_{0.13}O₂ material as

shown in Fig. 6b, shows an initial discharge capacity of ~ 212 mAh g⁻¹ and ~ 91 mAh g⁻¹ at 0.1 C and 2 C, respectively, validating the improvement in the electrochemical performance of SiO₂-coated materials. Moreover, 1.5 and 2.0 wt% SiO₂-coated materials also display improved rate performance when compared to uncoated Li_{1.2}Ni_{0.13}Mn_{0.54}Co_{0.13}O₂ material.

Figure 7 compares the rate capability performance of uncoated and SiO₂-coated Li_{1.2}Ni_{0.13}Mn_{0.54}Co_{0.13}O₂

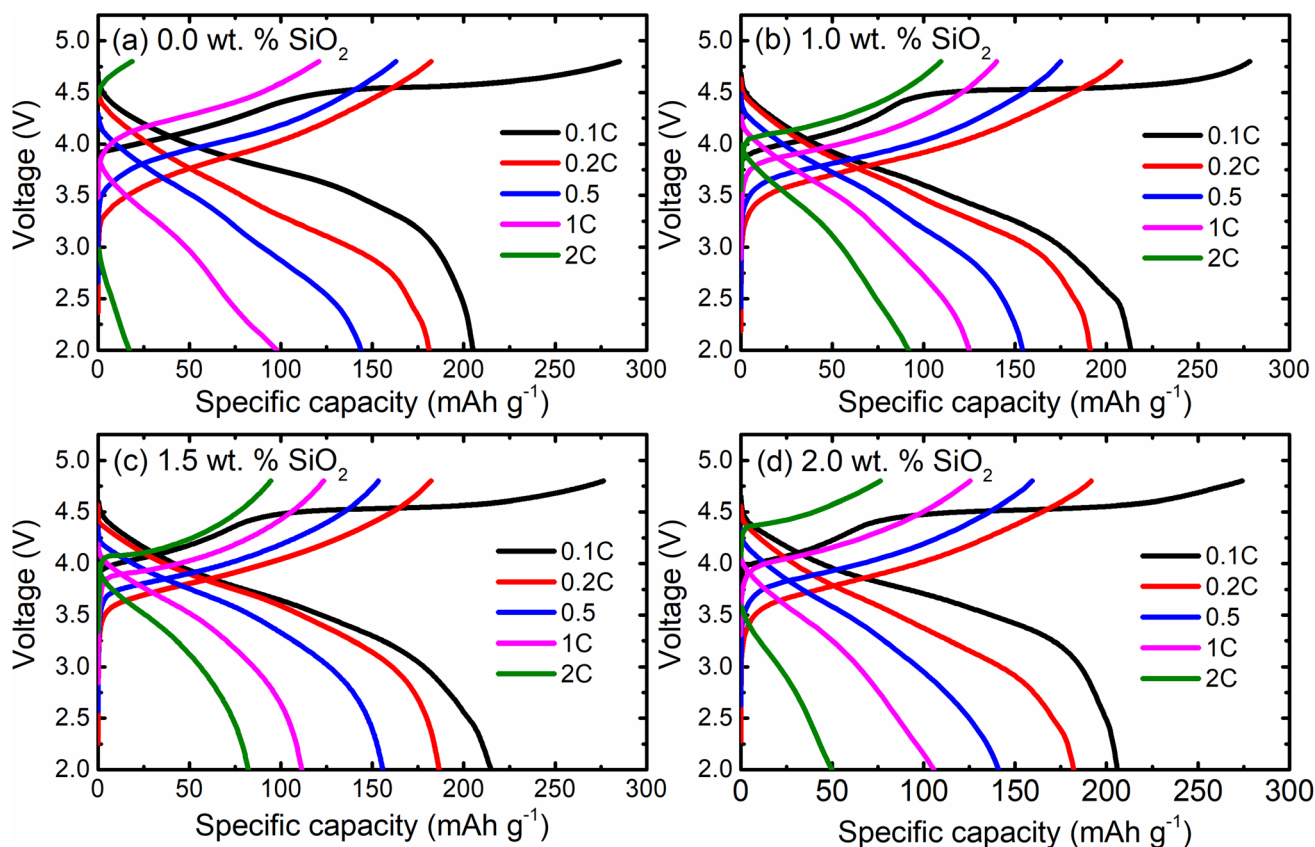


Fig. 6 Galvanostatic charge/discharge curves **a** uncoated **b–d** SiO₂-coated Li_{1.2}Ni_{0.13}Mn_{0.54}Co_{0.13}O₂ (SiO₂ = 1.0, 1.5 and 2.0 wt%) at various C-rates

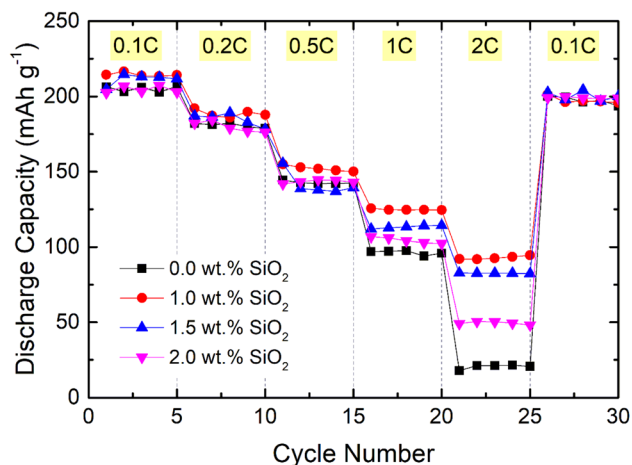


Fig. 7 Rate capability of uncoated and SiO₂-coated Li_{1.2}Ni_{0.13}Mn_{0.54}Co_{0.13}O₂ (SiO₂ = 1.0, 1.5 and 2.0 wt%) materials

materials at various C-rates. Uncoated material shows rapid capacity fading, especially at higher C-rates. On the other hand, SiO₂-coated materials display an improved rate capability performance. At

low C-rates, almost all the materials show very similar discharge capacity; however, at higher C-rate, the coated materials display higher capacity and better rate performance. The uncoated materials show the discharge capacity of around 100 mAh g⁻¹ and 16 mAh g⁻¹ at 1 C and 2 C, respectively. Whereas, all SiO₂-coated materials display higher discharge capacity at 1 C and 2 C. The improvement in capacity is quite prominent in the case of 1 wt% SiO₂-coated Li_{1.2}Ni_{0.13}Mn_{0.54}Co_{0.13}O₂ material. The 1 wt% SiO₂-coated Li_{1.2}Ni_{0.13}Mn_{0.54}Co_{0.13}O₂ materials demonstrate the best rate capability performance and display capacity of ~ 125 mAh g⁻¹ and ~ 93 mAh g⁻¹ at 1 C and 2 C, respectively. Usually, during high voltage operations, the electrode in de-lithiated states are quite unstable and rapidly reacts with electrolytes which result in degradation of battery performance. These types of surface coating are known to prevent the direct contact of electrolyte and cathode materials which helps to reduce the unwanted side reaction between them. It can be further noticed from Fig. 6 that increasing the coating amount from 1 wt% to 1.5

wt% and 2.0 wt% leads to decreasing discharge capacities. The main reason for the decrease in initial discharge capacity can be related to increased interfacial resistance due to the presence of in-active coating layer. This has been well understood and reported in several previous studies [11, 40, 43, 46]. Table 2 lists the discharge capacities of uncoated and SiO₂-coated Li_{1.2}Ni_{0.13}Mn_{0.54}Co_{0.13}O₂ material at various C-rates.

The cycling performance at 0.1 C for 50 cycles for uncoated and SiO₂-coated Li_{1.2}Ni_{0.13}Mn_{0.54}Co_{0.13}O₂ (SiO₂ = 1.0, 1.5 and 2.0 wt%) materials is shown in Fig. 8. It is observed that all the materials show slow capacity fading till 50 cycles. However, the uncoated Li_{1.2}Ni_{0.13}Mn_{0.54}Co_{0.13}O₂ material shows a relatively faster capacity fading when compared to SiO₂-coated Li_{1.2}Ni_{0.13}Mn_{0.54}Co_{0.13}O₂ (SiO₂ = 1.0, 1.5 and 2.0 wt%) materials. Figure 8b–e show the charge/discharge curves of uncoated and SiO₂-coated Li_{1.2}Ni_{0.13}Mn_{0.54}Co_{0.13}O₂ materials at different cycle numbers. It can be clearly seen that the synthesized material displays fast voltage degradation upon cycling, which is the inherent issue with this material. However, the SiO₂-coated Li_{1.2}Ni_{0.13}Mn_{0.54}Co_{0.13}O₂ materials show relatively slower voltage and capacity degradation, as seen in Fig. 8b–e. This voltage and capacity decay is generally due to the unstable crystal structure; however, with SiO₂ coating, the surface structure is protected, which prevents phase transformation upon cycling. The uncoated sample shows an initial discharge capacity of ~ 200 mAh g⁻¹, which decreases to ~ 160 mAh g⁻¹ after 50 cycles with the capacity retention of ~ 71%.

On the other hand, the SiO₂-coated Li_{1.2}Ni_{0.13}Mn_{0.54}Co_{0.13}O₂ materials show improved capacity retention. It can be observed that 1.0 wt% SiO₂-coated

material displayed the best initial discharge capacity. However, with increasing the thickness of the coating layer, the initial discharge capacity is slightly decreased, which might be due to increased interfacial resistance. Overall, SiO₂-coated Li_{1.2}Ni_{0.13}Mn_{0.54}Co_{0.13}O₂ materials exhibit improved cycling performance when compared with uncoated materials.

Figure 9 shows the thermal stability of uncoated and SiO₂-coated Li_{1.2}Ni_{0.13}Mn_{0.54}Co_{0.13}O₂ materials. It can be seen from the DSC results that all the materials are stable till 215 °C (on average). However, they show strong exothermic peaks beyond this temperature. Uncoated Li_{1.2}Ni_{0.13}Mn_{0.54}Co_{0.13}O₂ shows a strong exothermic peak at around 217.84 °C, which corresponds to the reaction between the charged cathode and the electrolyte solution. It is interesting to note that the thermal stability behavior of SiO₂-coated Li_{1.2}Ni_{0.13}Mn_{0.54}Co_{0.13}O₂ improved in terms of onset temperature and heat generation. The onset temperature for 1.0 wt% SiO₂ material is almost similar to uncoated material. However, the amount of heat generation decreased to a considerable amount for 1.0 wt% SiO₂ material. Moreover, the onset temperatures for 1.5 and 2.0 wt% SiO₂ materials increased to around 245 °C. Nevertheless, it can be noticed that heat generation for 2.0 wt% material has increased. Higher onset temperature might have resulted in the severe condition, which results in more heat generation once the exothermic reaction between the charged electrode and electrolyte initiated. Table 3 compares the onset temperatures and heat generations of uncoated and SiO₂-coated Li_{1.2}Ni_{0.13}Mn_{0.54}Co_{0.13}O₂ materials. The onset temperatures and heat generation trends have also been shown in Fig. S-3.

Table 2 Discharge capacities of uncoated and uncoated and SiO₂-coated Li_{1.2}Ni_{0.13}Mn_{0.54}Co_{0.13}O₂ (SiO₂ = 1.0, 1.5 and 2.0 wt%) materials at various C-rates

Materials/C-rate	0.1 C (mAh g ⁻¹)	0.2 C (mAh g ⁻¹)	0.5 C (mAh g ⁻¹)	1 C (mAh g ⁻¹)	2 C (mAh g ⁻¹)
0.0 wt% SiO ₂	205	182	142	97	21
1.0 wt% SiO ₂	214	185	152	125	93
1.5 wt% SiO ₂	213	189	138	114	83
2.0 wt% SiO ₂	203	179	144	104	50

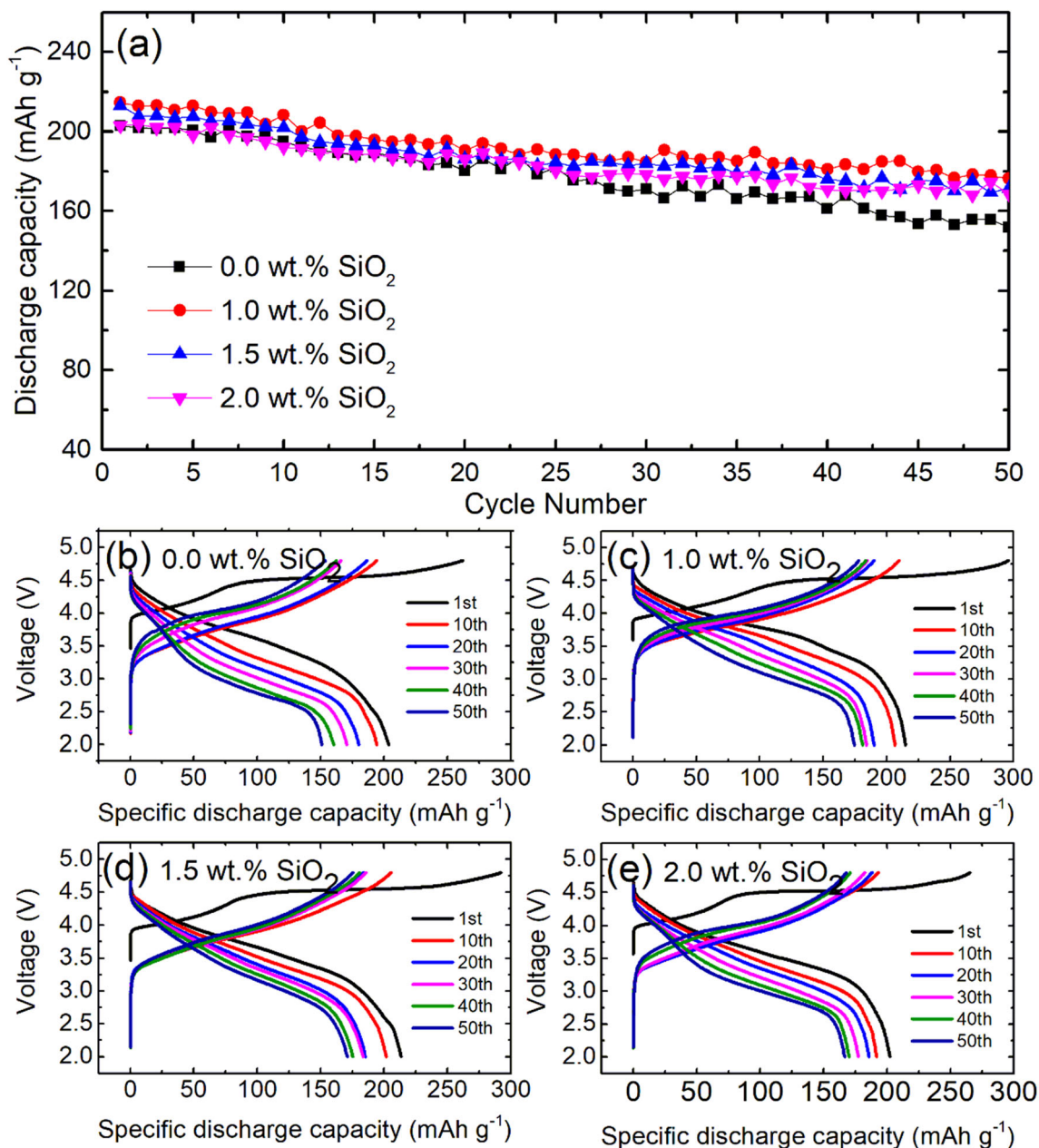


Fig. 8 Cycling behavior of uncoated and SiO₂-coated Li_{1.2}Ni_{0.13}Mn_{0.54}Co_{0.13}O₂ (SiO₂ = 1.0, 1.5 and 2.0 wt%) materials at 0.1 C for 50 cycles

4 Conclusions

The lithium-rich layered oxide (LLO) cathode was synthesized and coated with silica (SiO₂) to form SiO₂-coated Li_{1.2}Ni_{0.13}Mn_{0.54}Co_{0.13}O₂ materials (SiO₂ = 1.0, 1.5 and 2.0 wt%). The XRD results suggest the synthesis of phase pure materials without the presence of any impurity phases. SEM/TEM and XPS

analysis confirmed the synthesis of nanometric sized particles and the presence of SiO₂ layer on the surface of the particle. The electrochemical study shows that SiO₂-coated Li_{1.2}Ni_{0.13}Mn_{0.54}Co_{0.13}O₂ materials demonstrate improved performance in terms of rate capability and cycling performance. Moreover, SiO₂-coated Li_{1.2}Ni_{0.13}Mn_{0.54}Co_{0.13}O₂ displayed improved thermal stability behavior when compared to

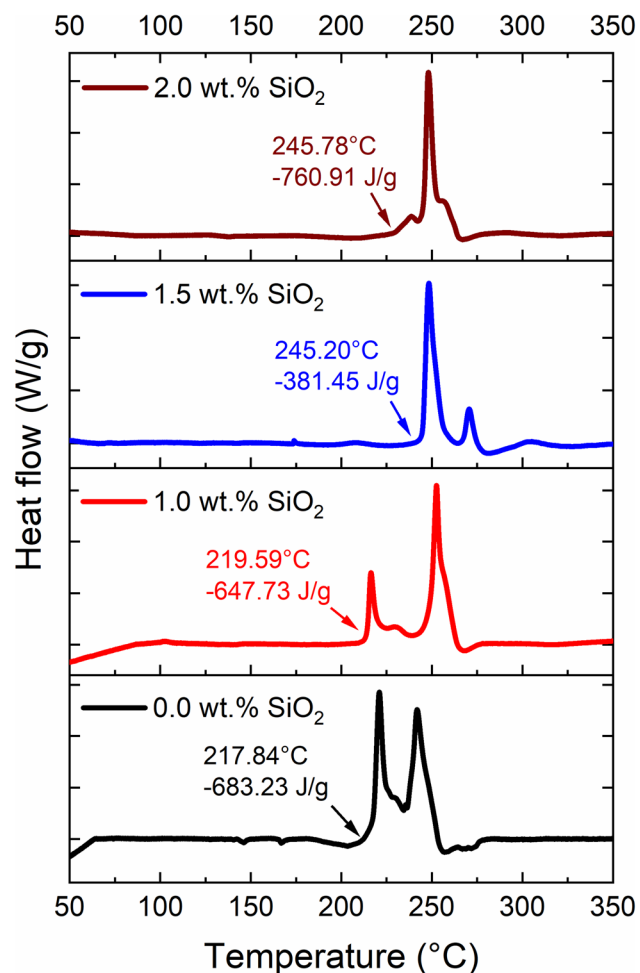


Fig. 9 DSC thermal stability profiles of uncoated and SiO₂-coated Li_{1.2}Ni_{0.13}Mn_{0.54}Co_{0.13}O₂ (SiO₂ = 1.0, 1.5 and 2.0 wt%) electrodes. The DSC measurements are taken by charging the electrodes to 4.7 V at 0.1 C

Table 3 DSC thermal stability of uncoated and SiO₂-coated Li_{1.2}Ni_{0.13}Mn_{0.54}Co_{0.13}O₂ materials

Sample	Onset temperature (°C)	Heat generation (J/g)
Uncoated	217.84	– 683.23
1.0 wt% SiO ₂	219.59	– 647.73
1.5 wt% SiO ₂	245.20	– 381.45
2.0 wt% SiO ₂	245.78	– 760.91

uncoated material. The improvement in electrochemical and thermal performance can be associated with the prevention of direct contact between cathode material and the electrolyte, which reduce the unwanted side reactions between them. However, the strategy of SiO₂ coating on

Li_{1.2}Ni_{0.13}Mn_{0.54}Co_{0.13}O₂ is quite effective and may pave the way for commercial battery materials coatings if effectively engineered.

Acknowledgements

This publication was made possible by NPRP Grant # NPRP11S-1225-170128 from Qatar National Research Fund (a member of the Qatar Foundation). Statements made herein are solely the responsibility of the authors. FE-SEM analysis was accomplished at the Central Laboratory Unit (CLU), Qatar University, Doha, Qatar, TEM analysis was conducted at the Core Labs., QEERI, HBKU, Qatar and XPS analysis was accomplished at the Gas Processing Center (GPC), Qatar University, Doha, Qatar.

Funding

Open Access funding provided by the Qatar National Library. NPRP11S-1225-170128 from Qatar National Research Fund.

Compliance with ethical standards

Conflicts of interest Not applicable

Electronic supplementary material: The online version of this article (<https://doi.org/10.1007/s10854-020-04481-6>) contains supplementary material, which is available to authorized users.

Open Access This article is licensed under a Creative Commons Attribution 4.0 International License, which permits use, sharing, adaptation, distribution and reproduction in any medium or format, as long as you give appropriate credit to the original author(s) and the source, provide a link to the Creative Commons licence, and indicate if changes were made. The images or other third party material in this article are included in the article's Creative Commons licence, unless indicated otherwise in a credit line to the material. If material is not included in the article's Creative Commons licence and your intended use is not permitted by statutory regulation or exceeds the permitted use, you will need to obtain permission directly from the copyright holder. To view a copy of this licence, visit <http://creativecommons.org/licenses/by/4.0/>.

References

1. M. Armand, J.-M. Tarascon, *Nature* **451**, 652 (2008)
2. V. Etacheri, R. Marom, R. Elazari, G. Salitra, D. Aurbach, *Energy Environ. Sci.* **4**, 3243 (2011)
3. S. Whittingham, *MRS Bull.* **33**, 411 (2008)
4. D. Larcher, J.-M. Tarascon, *Nat. Chem.* **7**, 19 (2015)
5. J.-M. Tarascon, *Philos. Trans. A. Math. Phys. Eng. Sci.* **368**, 3227 (2010)
6. D. Liu, F. Wang, G. Wang, C. Lv, Z. Wang, X. Duan, X. Li, *Molecules* **24**(9), 1680 (2019)
7. T. Cheng, Z. Ma, R. Gu, R. Chen, Y. Lyu, A. Nie, B. Guo, *Energies* **11**, 2712 (2018)
8. J.B. Goodenough, Y. Kim, *J. Power Sources* **196**, 6688 (2011)
9. W. Li, B. Song, A. Manthiram, *Chem. Soc. Rev.* **46**, 3006 (2017)
10. U. Nisar, R. Amin, R. Essehli, R.A. Shakoor, R. Kahraman, D.K. Kim, M.A. Khaleel, I. Belharouak, *J. Power Sources* **396**, 774 (2018)
11. U. Nisar, S.A.J.A. Al-Hail, R.K. Petla, R.A. Shakoor, R. Essehli, R. Kahraman, S.Y. AlQaradawi, D.K. Kim, I. Belharouak, M.R. Amin, *ACS Appl. Energy Mater.* **2**, 7263 (2019)
12. H. Yu, H. Zhou, *J. Phys. Chem. Lett.* **4**(8), 1268 (2013)
13. M.M. Thackeray, S.H. Kang, C.S. Johnson, J.T. Vaughey, R. Benedek, S.A. Hackney, *J. Mater. Chem.* **17**, 3112 (2007)
14. M.M. Thackeray, C.S. Johnson, J.T. Vaughey, N. Li, S.A. Hackney, *J. Mater. Chem.* **15**, 2257 (2005)
15. H. Yu, H. Kim, Y. Wang, P. He, D. Asakura, Y. Nakamura, H. Zhou, *Phys. Chem. Chem. Phys.* **14**, 6584 (2012)
16. H. Yu, H. Zhou, *J. Mater. Chem.* **22**, 15507 (2012)
17. H. Yu, Y. Wang, D. Asakura, E. Hosono, T. Zhang, H. Zhou, *RSC Adv.* **2**, 8797 (2012)
18. U. Nisar, R. Amin, A. Shakoor, R. Essehli, S. Al-Qaradawi, R. Kahraman, I. Belharouak, *Emergent Mater.* **1**, 155 (2018)
19. X. Lai, G. Hu, Z. Peng, H. Tong, Y. Lu, Y. Wang, X. Qi, Z. Xue, Y. Huang, K. Du, Y. Cao, *J. Power Sources* **431**, 144 (2019)
20. Y. Li, F. Lian, L. Ma, C. Liu, L. Yang, X. Sun, K. Chou, *Electrochim. Acta* **168**, 261 (2015)
21. R. Lin, E. Hu, M. Liu, Y. Wang, H. Cheng, J. Wu, J.C. Zheng, Q. Wu, S. Bak, X. Tong, R. Zhang, W. Yang, K.A. Persson, X. Yu, X.Q. Yang, H.L. Xin, *Nat. Commun.* **10**, 1 (2019)
22. B. Xu, C.R. Fell, M. Chi, Y.S. Meng, *Energy Environ. Sci.* **4**, 2223 (2011)
23. M. Gu, I. Belharouak, J. Zheng, H. Wu, J. Xiao, A. Genc, K. Amine, S. Thevuthasan, D.R. Baer, J.G. Zhang, N.D. Browning, J. Liu, C. Wang, *ACS Nano* **7**(1), 760 (2013)
24. M. Sathiyaa, A.M. Abakumov, D. Foix, G. Rousse, K. Ramesha, M. Saubanère, M.L. Doublet, H. Vezin, C.P. Laisa, A.S. Prakash, D. Gonbeau, G. Vantendeloo, J.M. Tarascon, *Nat. Mater.* **14**(2), 230 (2015)
25. Z. Wang, D. Santhanagopalan, W. Zhang, F. Wang, H.L. Xin, K. He, J. Li, N. Dudney, Y.S. Meng, *Nano Lett.* **6**(6), 3760 (2016)
26. F. Zheng, C. Yang, X. Xiong, J. Xiong, R. Hu, Y. Chen, M. Liu, *Angew. Chem. Int. Ed.* **54**, 13058 (2015)
27. K. Mu, Y. Cao, G. Hu, K. Du, H. Yang, Z. Gan, Z. Peng, *Electrochim. Acta* **273**, 88 (2018)
28. Y. Zhao, Z. Lv, T. Xu, J. Li, *J. Alloys Compd.* **715**, 105 (2017)
29. X. Zhang, I. Belharouak, L. Li, Y. Lei, J.W. Elam, A. Nie, X. Chen, R.S. Yassar, R.L. Axelbaum, *Adv. Energy Mater.* **3**, 1299 (2013)
30. H. Liu, D. Qian, M.G. Verde, M. Zhang, L. Baggetto, K. An, Y. Chen, K.J. Carroll, D. Lau, M. Chi, G.M. Veith, Y.S. Meng, *A.C.S. Appl. Mater. Interfaces* **7**, 19189 (2015)
31. S. Guo, H. Yu, P. Liu, X. Liu, D. Li, M. Chen, M. Ishida, H. Zhou, *J. Mater. Chem. A* **2**, 4422 (2014)
32. H. Liu, C. Chen, C. Du, X. He, G. Yin, B. Song, P. Zuo, X. Cheng, Y. Ma, Y. Gao, *J. Mater. Chem. A* **3**, 2634 (2015)
33. Q. Xie, C. Zhao, Z. Hu, Q. Huang, C. Chen, K. Liu, *RSC Adv.* **5**, 77324 (2015)
34. F. Wu, Z. Wang, Y. Su, N. Yan, L. Bao, S. Chen, *J. Power Sources* **247**, 20 (2014)
35. H. Li, H. Zhou, *Chem. Commun.* **48**, 1201 (2012)
36. Z. Chen, Y. Qin, K. Amine, *J. Mater. Chem.* **20**, 7606 (2010)
37. L.J. Fu, H. Liu, C. Li, Y.P. Wu, E. Rahm, R. Holze, H.Q. Wu, *Solid State Sci.* **8**, 113 (2006)
38. P. Guan, L. Zhou, Z. Yu, Y. Sun, Y. Liu, F. Wu, Y. Jiang, D. Chu, *J. Energy Chem.* **43**, 220 (2020)
39. U. Nisar, R. Petla, S.A.J. Al-hail, A.A. Quddus, H. Monawwar, A. Shakoor, R. Essehli, R. Amin, *RSC Adv.* **10**, 15274 (2020)
40. W. Cho, S.M. Kim, J.H. Song, T. Yim, S.G. Woo, K.W. Lee, J.S. Kim, Y.J. Kim, *J. Power Sources* **282**, 45 (2015)
41. Y. Da Li, S.X. Zhao, C.W. Nan, B.H. Li, *J. Alloys Compd.* **509**, 957 (2011)
42. S. Jiang, B. Zhao, Y. Chen, R. Cai, Z. Shao, *J. Power Sources* **238**, 356 (2013)
43. L.L. Zhang, G. Liang, G. Peng, F. Zou, Y.H. Huang, M.C. Croft, A. Ignatov, *J. Phys. Chem. C* **116**, 12401 (2012)
44. B. Liu, *Int. J. Electrochem. Sci.* **13**, 7578 (2018)
45. S. Shi, T. Wang, M. Cao, J. Wang, M. Zhao, G. Yang, *A.C.S. Appl. Mater. Interfaces* **8**, 11476 (2016)
46. D. Arumugam, G. Paruthimal Kalaignan, *J. Electroanal. Chem.* **624**, 197 (2008)

Publisher's Note Springer Nature remains neutral with regard to jurisdictional claims in published maps and institutional affiliations.